

The MACHO Project 2nd Year LMC Microlensing Results and Dark Matter Implications

M.R. Pratt^{a,b}, C. Alcock^{b,c}, R.A. Allsman^d, D. Alves^{c,e}, T.S. Axelrod^f, A.C. Becker^a, D.P. Bennett^{b,c,e}, K.H. Cook^{c,b}, K.C. Freeman^f, K. Griest^{g,b}, J. Guern^{g,b}, M.J. Lehner^{g,b}, S.L. Marshall^{b,c}, B.A. Peterson^f, P.J. Quinn^h, A.W. Rodgers^f, C.W. Stubbs^{a,b}, W. Sutherlandⁱ and D.L. Welch^j

^aAstronomy, Box 351580, University of Washington, Seattle, WA 98195-1580

^bCenter for Particle Astrophysics, University of California Berkeley, Berkeley, CA 94720

^cLawrence Livermore National Laboratory, Livermore, CA 94550

^dSupercomputing Facility, Australian National University, Canberra, ACT 0200, Australia

^eDepartment of Physics, University of California, Davis, CA 95616

^fMount Stromlo and Siding Springs Observatories, Australian National University, Weston, ACT 2611, Australia

^gDepartment of Physics, University of California San Diego, La Jolla, CA 92093-0350

^hEuropean Southern Observatory, Karl-Schwarzschild Str. 2, D-85748, Garching, Germany

ⁱDepartment of Physics, University of Oxford, Oxford OX1 3RH, U.K.

^jMcMaster University, Hamilton Ontario Canada L8S 4M1

The MACHO Project is searching for galactic dark matter in the form of massive compact halo objects (Machos). Millions of stars in the Large Magellanic Cloud (LMC), Small Magellanic Cloud (SMC), and Galactic bulge are photometrically monitored in an attempt to detect rare gravitational microlensing events caused by otherwise invisible Machos. Analysis of two years of photometry on 8.5 million stars in the LMC reveals 8 candidate microlensing events, far more than the ~ 1 event expected from lensing by low-mass stars in known galactic populations. From these eight events we estimate the optical depth towards the LMC from events with $2 < \hat{t} < 200$ days to be $\tau_2^{200} \approx 2.9_{-0.9}^{+1.4} \times 10^{-7}$. This exceeds the optical depth of 0.5×10^{-7} expected from known stars and is to be compared with an optical depth of 4.7×10^{-7} predicted for a “standard” halo composed entirely of Machos. The total mass in this lensing population is $\approx 2_{-0.7}^{+1.2} \times 10^{11} M_\odot$ (within 50 kpc from the Galactic center). Event timescales yield a most probable Macho mass of $0.5_{-0.2}^{+0.3} M_\odot$, although this value is quite model dependent.

1. INTRODUCTION

Galactic dark matter in the form of Machos can be detected by its occasional gravitational microlensing of extragalactic stars [1, 2, 3]. This effect occurs when a Macho of mass m is in close alignment with a background star and acts as a gravitational lens, magnifying and distort-

ing the stellar image. Microlensing refers to the situation in which image distortion is not detectable ($\ll 1$ arcsec) and the only visible effect is an apparent amplification, $A = (u^2 + 2)/u\sqrt{u^2 + 4}$. Here $u = b/r_E$ is the impact parameter in units of the Einstein radius $r_E = \sqrt{4GmD_{OL}D_{LS}/c^2D_{OS}}$ where D_{OL}, D_{LS} & D_{OS} are distances between observer, source and lens[

4]. This effect is transient with a timescale, $\hat{t} \equiv 2r_E/v_{\perp}$, set by the mass and location of the lens and its motion relative to the line of sight. For a source in the Magellanic Clouds and a lens at 10 kpc, $r_E \approx 8\sqrt{m/M_{\odot}}$ AU and $\hat{t} \approx 140\sqrt{m/M_{\odot}}$ days for $v_{\perp} = 200 \text{ km s}^{-1}$. With \sim daily observations over periods of years, Machos in the range $10^{-4} - 10^2 M_{\odot}$ are experimentally accessible.

Because the “area” of the lens is proportional to its mass, the fraction of solid angle occupied by lenses, τ , depends only on the mass density of Machos and not on their particular sizes. Application of the virial theorem shows that $\tau \sim (v_c/c)^2 \sim 5 \times 10^{-7}$ for a Macho-dominated halo. Here v_c is the circular velocity about the center of the galaxy. Thus detection of these very rare events requires many repeated observations of millions of sources. The optical depth towards the Magellanic Clouds due to a Macho-dominated halo still comfortably exceeds that from known populations of low-mass stars, so that microlensing surveys directly probe the Macho content of the halo.

Several groups are now engaged in large scale photometric surveys to search for dark matter in the form Machos using the high density of stars in in the Magellanic Clouds, M31 and the Galactic bulge as a backdrop for gravitational microlensing. Four such surveys, DUO, EROS, MACHO and OGLE, have detected in excess of 100 events that appear to be microlensing [5, 6, 7, 8, 9, 10, 11, 12, 13] of which ~ 10 are toward the LMC, the remainder being toward the Galactic bulge. Most of these events have characteristic timescales $\hat{t} \sim 20 - 60$ days. Searches for short-timescale events with 1 hour $\lesssim \hat{t} \lesssim 10$ days have revealed no candidates to date and set interesting limits on low-mass Machos [14, 15, 16]. Detailed reviews of microlensing are given by [17] and [18], a basic outline of the MACHO project, and analysis procedures is given in [12] (hereafter A96) and a more detailed analysis of this sample is found in [19].

2. OBSERVATIONS & PHOTOMETRY

The MACHO Project has had full-time use of the 1.27-meter telescope at Mount Stromlo Ob-

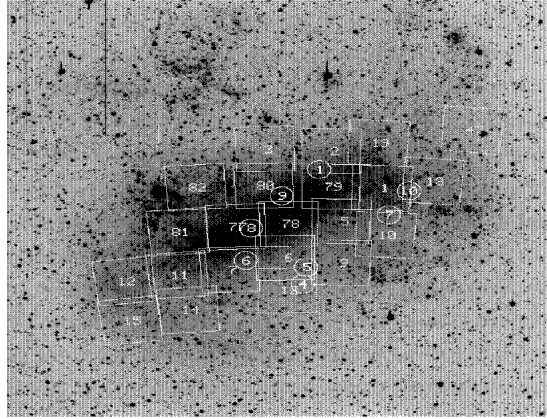


Figure 1. An R-band image of the LMC, 8.2 degrees on a side (G. Bothun, private communication), showing the locations of the 22 MACHO fields used here. Event locations are shown with circles.

servatory, Australia, since mid 1992 in an extended run until the end of the century. Details of the telescope system are given in [20] and of the camera system in [21, 22]. Briefly, corrective optics and a dichroic beam splitter are used to simultaneously image a 42×42 arcmin² field in two colors, using two mosaics of four 2048² pixel CCDs.

As of this writing, over 44000 exposures have been taken with the system, over 3 TBytes of raw image data. About 60% are of the LMC, the remainder are towards the Galactic bulge and SMC. In this paper, we consider only the first 2.1 years of data from 22 well-sampled LMC fields, located in the central $\sim 5^{\circ} \times 3^{\circ}$ of the LMC and shown in Figure 1.

The observations described here comprise 10827 images distributed over the 22 fields. These include observations over a time span of 840 days from mid 1992 to late 1994. The mean number of exposures per field is 492, with a range from 300 to 785. The sampling varies between fields

Table 1
Event selection criteria

	Description	Value
1	Coverage	$\dot{t} < 300$ days & $t_{\max} \in$ data range
2	Constant baseline	$\chi_{ml-out}^2/N_{\text{dof}} < 4$ with $N_{\text{dof}} > 40$
3	Amplification	$A_{\max} > 1 + 2\bar{\sigma}$
4	Significance	6 measurements $> 1\sigma$ high
5	Variable (Bumpers & very red stars)	$V > 17.5$ & $V - R < 0.9$
6	SN 1987A light echos	$10' \times 10'$ region excluded
7	Peak fit	$\Delta\chi^2/(\chi_{\text{peak}}^2/N_{\text{dof}}) > 200$
8	Crowding	$> 95\%$ of measurements have low crowding
9	Crowding	$f_{CRD} < 70 \log_{10}[\Delta\chi^2/(\chi_{ml}^2/N_{\text{dof}})] - 45$
10	Significance	$\Delta\chi^2/(\chi_{ml}^2/N_{\text{dof}}) > 500$
11	Amplification	$A_{\max} > 1.75$

since the higher priority fields were often observed twice per night with a ~ 4 hour spacing for sensitivity to very short timescale events[15, 16].

The photometric reduction procedure here is identical to that described in A96; briefly, a good-quality image of each field is chosen as a template, and used to generate a list of stellar positions and magnitudes. All other images are aligned with the template using fiducial stars, and a PSF is determined from these. Then, the flux of all other stars is fitted using the known positions and PSF. For each measurement we also compute an error estimate and six quality flags; these flags are the object type, the χ^2 of the PSF fit, a crowding parameter, a local sky estimate, and the fraction of the star’s flux rejected due to bad pixels and cosmic rays. Suspect measurements are removed based on these quality flags and the resulting data are organized into stellar lightcurves.

3. EVENT DETECTION

The MACHO Project is the largest survey of astronomical variability in history and as such encompasses many previously unknown backgrounds to microlensing. The data used here comprise some 9 billion photometric measurements. Although we use objective selection criteria (cuts) to discriminate genuine microlensing from stellar variability and systematic photometry errors, these cuts are developed after extensive examination of the MACHO database. However,

as long as the experiment’s event *detection efficiency* is calculated properly, and the selection criteria are sufficiently stringent to accept only real microlensing events, changes in the selection criteria will be accounted for in the efficiency calculations, and the details will not bias the final results.

Our experience with the Galactic bulge has been helpful in developing the current cuts. Since our previous analysis of a smaller set of LMC data (A96), we have analyzed a large set of data towards the Galactic bulge [9, 10], which has yielded over 80 microlensing events. These observations provide a more realistic set of microlensing events than the artificial events we previously used to test our analysis procedures. A number of these events fail the original cuts because they are not well described by the “normal” microlensing light curve which assumes a single point lens, constant velocities, and an unblended source star but nevertheless appear by eye to be very high quality microlensing events. In contrast events 2 and 3 of A96 appear far less striking.

This has motivated us to modify our selection criteria, shown in Table 1, to have less stringent requirements on the functional form of the lightcurve. We compensate for this by demanding higher signal to noise *i. e.* higher amplification and greater statistical significance.

Event detection proceeds in several stages. In the first stage, the lightcurves of §2 are convolved with 7, 15 and 45 day matched filters as in

A96 and low level triggers are fit with the “standard” microlensing curve $A(u(t))$, where $u(t) = \sqrt{u_{\min}^2 + 4(t - t_{\max})^2/\hat{t}^2}$. We then compute for each light curve a set of statistics and apply the cuts shown in Table 1 to distinguish microlensing from the background. A measure of significance is $\Delta\chi^2/(\chi_{ml}^2/N_{\text{dof}})$, where $\Delta\chi^2 \equiv \chi_{\text{const}}^2 - \chi_{ml}^2$ is the improvement in χ^2 between a constant brightness fit and a microlensing fit.

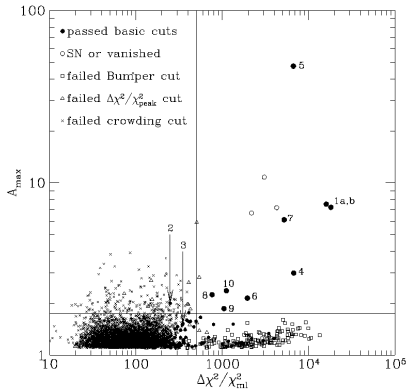


Figure 2. The final cuts for selection of microlensing candidates. The y-axis is the fit A_{\max} . The solid lines show the final cuts 10 and 11; the circles in the upper right are the 12 events (10 stars) passing all cuts.

Two of the principal cuts are summarized in Figure 2, which illustrates cuts 10 and 11 for all events that pass cuts 1-4 & 6. Events that pass all cuts are indicated with circles, while the other open symbols and crosses indicate events which failed 1 or more of cuts 5 & 7-9.. Open squares indicate events which fail cut 5 on magnitude, and open triangles indicate events which fail cut 7 on peak fit. The crosses indicate events which fail cuts 8 or 9. The lightcurves passing all of these selection criteria are further investigated,

as outlined below.

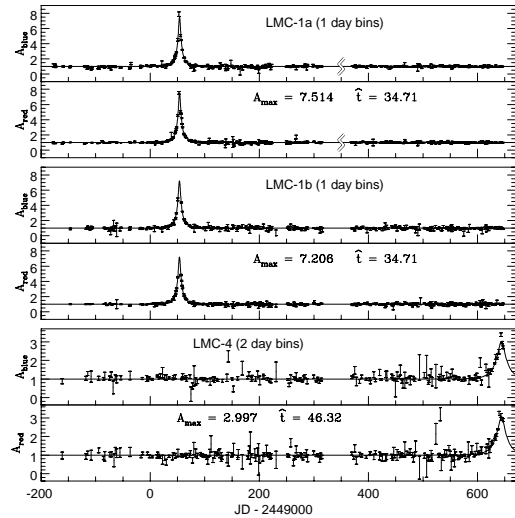


Figure 3. Candidate lightcurves 1 & 4

4. MICROLENSING CANDIDATES

Twelve lightcurves pass the cuts discussed above, indicated by the large open and filled circles in the upper right hand region of Figure 2. Some lightcurves are shown in Figures 3 & 4 and event fit parameters are listed in Table 2. Four of these lightcurves (1a, 1b, 12a and 12b) correspond to stars which occur in field overlap regions; the two lightcurves for each star are based on independent data and reductions and are detected independently.

Event 1 was our first discovery [5], and has remained constant in following years. The star’s spectrum is that of a normal clump giant at the radial velocity of the LMC [23].

The low signal-to-noise candidates 2 and 3 from A96 **do not pass** the final cuts used for this data set and are not included in following calculations, but we have numbered the present set of 10 candidates 1, 4... 12 to avoid possible ambiguity. The EROS group has informed us that the star involved in event 2 may have brightened in 1990,

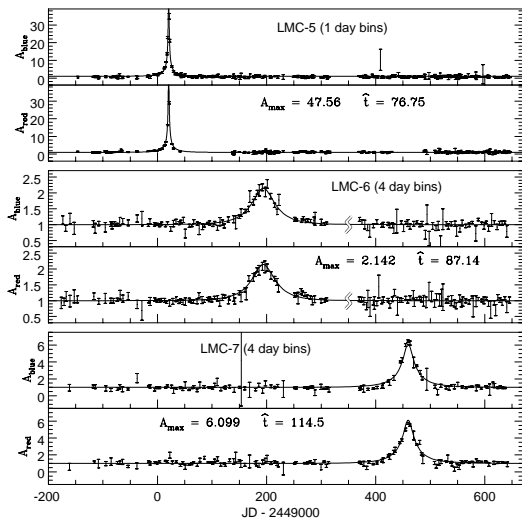


Figure 4. Candidate lightcurves 5-7

and it has also shown indication of further brightening episodes in our subsequent data; thus it is probably a variable star.

Event 4 was the first LMC microlensing candidate detected in progress by our real-time Alert system [10] and announced in IAU Circular 6095. This event is confirmed by additional photometry and spectra, obtained near peak amplification [24].

Event 9 passes our objective data cuts, but it appears to be lensing by a binary system. This event may resolve the extended size of the source star, providing a measure of the relative proper motion of the lens and source, which indicates the lens may reside in the LMC [25].

Event 10 passes all of our cuts, but our experience suggests that it may be a variable star. The asymmetry seen in the light curve, a rapid rise with a more gradual fall, is typical behavior one expects from variable stars.

Events 11 and 12a/b are indicated with open circles in Figure 2 as they are only present in our reference template images because of their amplification during that particular observation. They are no longer detectable in images that go somewhat deeper. Event 11 is superimposed on a

background galaxy and is almost certainly a supernova in that galaxy. Event 12 may in fact be microlensing. Our efficiency analysis, described below, does not take into account this “amplification bias” therefore it is necessary to discard both of these events for the following calculations.

These events, as shown in Figure 1, do not cluster spatially or in any particular stellar population. In addition, the distribution of fit A_{\max} is consistent with the expected uniform distribution of u_{\min} . We classify events 1,4,5 & 9 as ‘excellent’ microlensing candidates, events 6-8 as ‘good’ and event 10 as ‘marginal’. Events 11 & 12 must be rejected as explained above, and events 2 & 3 from A96 do not pass the current cuts. We define two sets of events for the following analysis. The first set contains all eight events passing the cuts without amplification bias. The second, more conservative, set of 6 events eliminates event 9 as a possible LMC lens and event 10 as a possible variable star.

5. DETECTION EFFICIENCY

The detection probability for individual events depends on many factors, e.g. the 3 event parameters A_{\max} , \hat{t} , t_{\max} , and the unlensed stellar magnitude, as well as our observing strategy and weather conditions. However, we can average over the known distributions of A_{\max} and t_{\max} and stellar magnitude, using the known time-sampling and weather conditions, to derive our efficiency, shown in Figure 5, as a function only of event timescale $\mathcal{E}(\hat{t})$.

We have computed our detection efficiency using an essentially identical method to that outlined in A96, simply generating simulated microlensing events with \hat{t} logarithmically distributed in the range 0.3–1000 days and adding these simulated events into the extended timespan of observations. The Monte-Carlo procedure takes into account the actual spacing and error bars of the observations, so any variations in sampling frequency, weather, seeing etc. between the first and second year data are automatically accounted for.

Efficiency is defined as the fraction of input events with $u_{\min} < 1$ which pass our cuts; since

Table 2
Event parameters & contribution to τ

Event	V	V-R	t_{\max}	\hat{t}	A_{\max}	χ^2/N_{dof}	\hat{t}_{bl}	τ_1
1a	19.6	0.6	57.08(3)	34.7(3)	7.2(1)	1.420	38.8	1.8×10^{-8}
1b	19.6	0.6	57.26(4)	34.3(3)	7.5(3)	1.134		
4	20.0	0.2	647.2(2)	46(2)	3.00(4)	1.416	52	2.3×10^{-8}
5	20.7	0.4	24.0(3)	82(2)	58(5)	1.680	88	3.5×10^{-8}
6	19.6	0.3	197.5(7)	87(4)	2.14(4)	0.873	100	4.1×10^{-8}
7	20.7	0.4	463.0(3)	115(3)	6.16(10)	1.447	131	6.0×10^{-8}
8	20.1	0.3	388.4(5)	62(2)	2.24(5)	2.218	70	2.8×10^{-8}
9 ¹	19.3	0.3	603.04(2)	143.4(2)	()	1.755	143	6.6×10^{-8}
10	19.4	0.2	205.3(3)	42(1)	2.36(5)	1.982	47	2.1×10^{-8}
11	21.5	0.4	-8.6(3)	266(9)	11.9(4)	2.964		
12a	21.2	0.3	-10.0(3)	138(5)	7.2(4)	1.487		
12b	21.2	0.3	-11.4(8)	162(8)	6.8(2)	1.536		

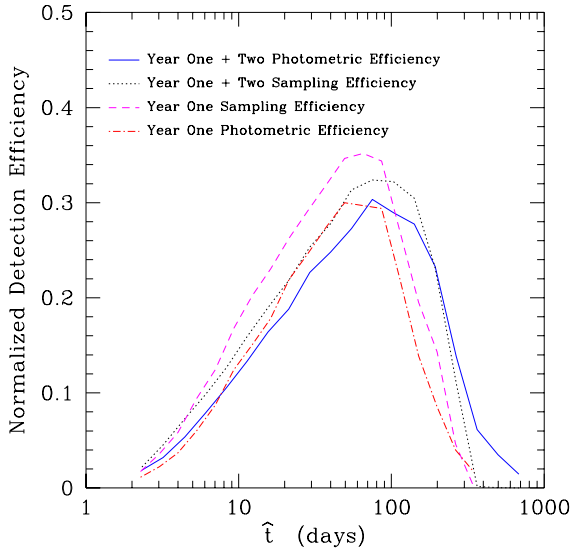


Figure 5. Microlensing detection efficiency (normalized to $u_{\min} < 1$) for the 2-year Macho data, as a function of event timescale \hat{t} .

we use a cut of $A_{\max} > 1.75$ or $u_{\min} < 0.661$, our efficiency is constrained to be less than 0.661. This efficiency is defined relative to an ‘exposure’ of $E = 1.82 \times 10^7$ star-years, which arises from the 7.9 million well measured, independent lightcurves in our sample multiplied by the 840-day span of observations.

We calculate our efficiency with two levels of

realism. The first is the ‘sampling’ efficiency, in which we neglect stellar blending and assume that all the additional flux in a microlensing event is recovered by the photometry code. The second is the ‘photometric’ efficiency, where we add artificial stars to a representative set of real images, rerun the photometry code to create look-up tables of added vs. recovered flux. These look-up tables are then used to generate artificial microlensing lightcurves in the same way as above. This ‘photometric’ efficiency is more realistic, and is typically $\sim 20\%$ lower than the ‘sampling’ efficiency for timescales less than 200 days.

The photometric efficiency is based on all stars in our fields, even those not uniquely identified because of S/N or crowding effects. These are accounted for by integrating the detection efficiency per star over a corrected luminosity function (LF) as in A96. This corrected LF is truncated about one magnitude beyond where our measured LF becomes seriously incomplete. However, the real LF continues to rise as $10^{0.5m}$ for several magnitudes beyond this cutoff so there should be an additional contribution to our exposure from these fainter stars. We have tried several different magnitude cutoffs and it appears that our exposure ($E\mathcal{E}$) is converging near the cutoff used in this paper for events with $\hat{t} < 150$ days.

In the photometric efficiency Monte Carlo, we find that in addition to reducing our efficiency, extreme crowding tends to make events appear

lower amplitude and shorter. This effect is due to “blending” or the tendency of a group of several superimposed stars to be detected as a single object. We make statistical corrections for this effect in column 8 of Table 2. Our estimated systematic error in the efficiency determination is $\sim 10\%$, less than our statistical error with eight events [19].

The efficiency for timescales $\hat{t} \sim 10 - 60$ days is lower than that from A96 by $\sim 10\%$ primarily because of the tighter A_{\max} and $\Delta\chi^2$ cuts. For longer events, the two year data is more sensitive because of its longer time span.

6. OPTICAL DEPTH

The simplest measurable quantity in a gravitational microlensing experiment is the microlensing optical depth. In the limit $\tau \ll 1$, this is the instantaneous probability that a random star is magnified by a lensing object by more than a factor of 1.34 ($u_{\min} < 1$). This is related to the mass in microlensing objects along the line of sight to the source stars by

$$\tau = \frac{4\pi G}{c^2} \int \rho(l) \frac{l(D_{OS} - l)}{D_{OS}} dl \quad (1)$$

Thus, it depends only on the density profile of lenses, not on their masses or velocities. Experimentally, one can obtain an unbiased estimate of the optical depth as

$$\tau_{\text{meas}} = \frac{1}{E} \frac{\pi}{4} \sum_i \frac{\hat{t}_i}{\mathcal{E}(\hat{t}_i)}. \quad (2)$$

where E is the total exposure (in star-years), \hat{t}_i is the Einstein ring diameter crossing time, and $\mathcal{E}(\hat{t}_i)$ is the detection efficiency. Here, and below, we use the blend corrected values, \hat{t}_{bl} , from column 8 of Table 2.

Confidence levels on τ_{meas} are determined from Monte Carlo experiments, in which the number of events is a Poisson variable with adjustable mean, and event timescales are drawn at random from the observed set. The mean is fixed so that 16% of experiments yield an optical depth larger/smaller than that measured. The mean optical depth for these experiments is then the “ 1σ ” lower/upper bound on τ_{meas} .

Using our full sample of 8 events, we find an optical depth for events of duration 2 days $< \hat{t} < 200$ days of $\tau_2^{200} = 2.9_{-0.9}^{+1.4} \times 10^{-7}$. If we subtract the predicted background microlensing optical depth of $\tau_{\text{backgnd}} = 0.5 \times 10^{-7}$ (from Table 3 below), we find that the observed excess is about 50% of the predicted microlensing optical depth for a “standard” all-Macho halo of e.g. [3]. Alternatively, we can estimate the optical depth due only to the halo by using the 6 event subsample defined in section 3, for which $\tau_2^{200} = 2.1_{-0.7}^{+1.1} \times 10^{-7}$, about 45% of the optical depth predicted by a “standard” all-Macho halo.

Uncertainties can be much larger than those calculated above if our measured distribution of timescales is a poor estimate of the real timescale distribution, especially if very long events are possible. It is worth noting that errors are considerably larger than Poisson because they are dominated by the shot noise on the small number of long events rather than the total number of events.

7. NON-HALO POPULATIONS

An in depth assessment of the microlensing background is necessary to determine if τ_{meas} and N_{meas} are significantly greater than that expected from non-halo populations. As noted by [26, 27, 28] and A96, low-mass stars in the Galaxy and LMC will give rise to some microlensing events. However, these authors find that the optical depth from known stars is only $\lesssim 10\%$ of that from an all-Macho halo.

Shown in Table 3 are estimates of stellar lensing rates of A96, using the same model parameters for the thin and thick disks, the spheroid and the LMC disk, assuming a Scalo PDMF for all populations, and simply updating the total exposure for our 2-year dataset. In our present sample, we expect a total background of 1.14 events from all known stellar populations.

A Poisson distribution with a mean of 1.14 gives probabilities to observe $N_{\text{obs}} \geq 3, 4, 5, 6, 7$ as 10.7%, 2.9%, 0.6%, 0.11%, 0.02% respectively. Thus we see that if only three of our events are genuine microlensing, the evidence for an excess is modest, whereas if more than four of our events

Table 3
Microlensing by stars

Population	$\tau(10^{-7})$	$\langle \hat{t} \rangle$ (days)	$\langle l \rangle$ (kpc)	$\Gamma(10^{-7}\text{yr}^{-1})$	N_{exp}
Thin disk	0.15	112	0.96	0.62	0.29
Thick disk	0.036	105	3.0	0.16	0.075
Spheroid	0.029	95	8.2	0.14	0.066
LMC center	0.53	93	49.8	2.66	(1.19)
LMC average	0.32	93	49.8	1.60	0.71
Standard halo	4.7	89	14.4	24.3	11.2

are microlensing there is very strong evidence for an excess over stellar lensing alone.

If one supposes that only the four “best” events result from lensing by stars and the other candidates are not microlensing (e.g. they are variable stars) then there is only marginal evidence for Machos in the halo. The flaw in this argument is that the distribution of microlensing magnifications is given *a priori*, and the “best” microlensing candidates are preferentially the high magnification ones. We should expect to find a mixture of high and low magnification candidates, and it is very unlikely that all events would be high magnification given our detection efficiency. By this argument, the surplus of events is not critically dependent on the lower quality candidates and it is difficult to explain our results by stellar lensing alone.

8. LIKELIHOOD ANALYSIS

Since the timescale of a lensing event is proportional to \sqrt{m} , we may use the observed event timescales to estimate the lens masses, given a particular halo model to fix the phase space distribution of lenses. We apply a maximum-likelihood method as in A96 using the “standard” halo where a fraction f of the dark halo is made of Machos with a unique mass m (the remaining $1-f$ of the halo is assumed to be unobserved dark matter). The resulting likelihood contours, assuming a delta-function mass function, are shown in Figure 6; the probabilities are computed using a Bayesian method with a prior uniform in f and $\log m$. The peak of the likelihood contours gives the most probable mass and halo fraction for this halo model. For the 6 event sample we

find $m_{2D} = 0.41 M_{\odot}$, and $f_{2D} = 0.51$.

We calculate one-dimensional likelihoods by integrating over the other parameter. For the six event sample this yields a most likely Macho mass $m = 0.46_{-0.17}^{+0.30} M_{\odot}$, and most likely halo fraction $f = 0.50_{-0.20}^{+0.30}$. The errors given are 68% CL. It is important to note the large extent of the contours in Figure 6. This is mostly due to the small number of events. The 95% CL contour includes halo fractions from 17% to 100%, and Machos masses from 0.12 to $1.2 M_{\odot}$.

The most probable mass and halo fraction are both larger than our results from year-1, which were $m = 0.06 M_{\odot}$ and $f = 0.2$, though there is a reasonable degree of overlap of the contours. The year-1 90% CL contour is shown as the light line in Figure 6. The most probable value of each analysis lies outside the 90% CL contour of the other analysis. This is primarily due to the upward shift in $\langle \hat{t} \rangle$. Events 2 & 3 from A96, dropped in this analysis, are both shorter than any events in the current set. The shift in $\langle \hat{t} \rangle$ is also to be expected as our maximum efficiency shifts toward longer events with the increasing baseline of the experiment.

9. DISCUSSION

One natural explanation of the results presented here is that a substantial fraction of the Galactic dark halo is in the form of Machos. The fact that the observed events have relatively long timescales suggests that (for canonical halo models) the lenses have masses above $\sim 0.1 M_{\odot}$, with a most probable mass $\sim 0.5 M_{\odot}$. If so, they cannot be ordinary hydrogen-burning stars since there are strong direct limits on such objects from

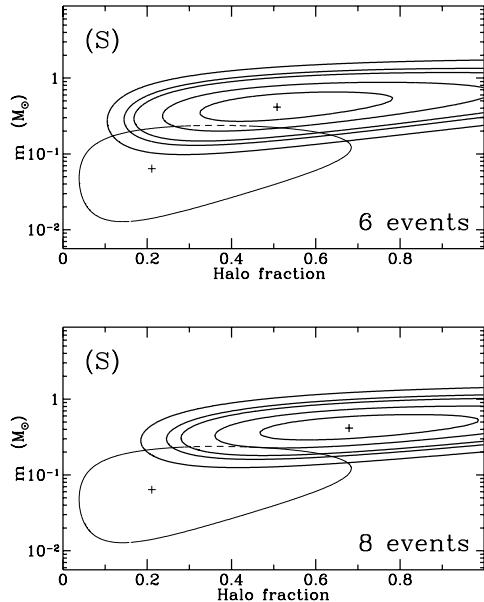


Figure 6. Likelihood contours of Macho mass m and halo Macho fraction f for a delta-function mass distribution, for halo model S. The most likely value is indicated with a +, and the contours enclose total probabilities of 34%, 68%, 90%, 95%, 99%, using a Bayesian method as described in § 8. The light line shows the 90% contour from A96.

counts of faint red stars (e.g. [29, 30, 31]); thus stellar remnants such as white dwarfs appear to be an obvious possibility.

There are some theoretical difficulties with the white-dwarf hypothesis (e.g. [32, 33]). First, the initial mass function must be fairly sharply peaked between $\sim 2 - 6 M_{\odot}$ to avoid overproducing either low-mass stars (which survive to the present) or high-mass stars (which as type-II SNe overproduce metals). A second difficulty is that the high luminosity of the B and A progenitors may exceed the observed faint galaxy counts.

However, white dwarfs are one of the few dark matter candidates which are known to exist in large numbers. Also, it has recently become clear (e.g. [34]) that the mass of hot gas in rich galaxy clusters greatly exceeds that in stars, and furthermore this gas is relatively metal-rich with an iron abundance ~ 0.3 solar. This might suggest that

most of the baryons have been processed through massive stars, which have since died leaving a population of remnants and metal-rich gas. This scenario has been explored by [35], who suggest that it may be natural to have 40-100% of the Galactic dark matter in white dwarfs.

The observational limits on the local density of white dwarfs are a strong function of their age [36, 37]. Very recently, a limit from the Hubble Deep Field has been given by [31]; they find that white dwarfs with $M_I < 16$ contribute $< 100\%$ of the halo density, and those with $M_I < 15$ contribute $< 33\%$.

Our exploration of halo models also shows that for ‘minimal’ halos, the timescales may still be consistent with substellar Machos just below $0.1 M_{\odot}$. Also, models with a substantial degree of halo rotation may lead to smaller mass estimates, since the rotation could reduce the transverse component of the Macho velocities. Thus, brown dwarfs cannot be ruled out as yet.

Finally, it is worth noting that microlensing is sensitive to any compact objects, irrespective of composition, as long as they are smaller than their Einstein radii. Thus, more exotic objects such as primordial black holes and strange stars are possible candidates that are virtually undetectable by direct searches.

The most direct method for identifying the lens population is to measure microlensing ‘parallax’ by simultaneously observing events from earth and a small telescope in Solar orbit [38]. This measures the velocity of the lens projected to the Solar system, which provides a definitive proof of microlensing, and discrimination between disk, halo and LMC lenses on an event-by-event basis.

To summarize, our results indicate a microlensing optical depth of $\approx 3 \times 10^{-7}$ or a Macho mass within 50 kpc of $\approx 2 \times 10^{11} M_{\odot}$. This provides evidence that Machos with masses in the range $0.05 - 1 M_{\odot}$ contribute a substantial fraction of the galactic dark halo. Continued observations from this and other projects should clarify this in the next few years.

10. ACKNOWLEDGMENTS

We are very grateful for the skilled support given our project by S. Chan and the technical staff at the Mt. Stromlo Observatory. Work performed at LLNL is supported by the DOE under contract W-7405-ENG. Work performed by the Center for Particle Astrophysics personnel is supported by the NSF through AST 9120005. The work at MSSSO is supported by the Australian Department of Industry, Science, and Technology., K.G. acknowledges support from DoE OJI, Alfred P. Sloan, and Cotrell Scholar awards. C.S. acknowledges the generous support of the Packard, Sloan and Seaver Foundations.

REFERENCES

1. M. Petrou. PhD thesis, University of Cambridge, 1981.
2. B Paczyński. *ApJ*, 304:1, 1986.
3. K. Griest. *ApJ*, 366:412, 1991.
4. S. Refsdal. *MNRAS*, 128:295, 1964.
5. C. Alcock et al. *Nature*, 365:621, 1993.
6. E. Aubourg et al. *Nature*, 365:623, 1993.
7. A. Udalski et al. *Acta Astronomica*, 43:289, 1993.
8. A. Udalski et al. *Acta Astronomica*, 44:165, 1994.
9. C. Alcock et al. *ApJ*, 1996. Submitted (astro-ph/9512146).
10. M.R. Pratt et al. In C. S. Kochanek and J. N. Hewitt, editors, *Astrophysical Applications of Gravitational Lensing*. Kluwer Academic Publishers, 1995. (astro-ph/9508039).
11. C. Alard, S. Mao, and J. Guibert. *A&A*, 300:L17, 1996.
12. C. Alcock et al. *ApJ*, 461:84, 1996.
13. C. Alcock et al. *Phys. Rev. Lett.*, 74:2867, 1995.
14. E. Aubourg. et al. *A&A*, 301:1, 1995.
15. C. Alcock et al. *ApJ*, 1996. Submitted (astro-ph/9604176).
16. M. Lehner et al. In *these proceedings*, 1996.
17. B. Paczyński. *ARA&A*, 1996. In press.
18. E. Roulet and S. Mollerach. 1996. In press (astro-ph/9603119).
19. C. Alcock et al. *ApJ*, 1996. In Preparation.
20. J. Hart et al. *PASP*, 108:220, 1996.
21. C.W. Stubbs et al. In M. Blouke, editor, *Charge Coupled Devices and Solid State Optical Sensors III*, volume 1900 of *Proceedings of the SPIE*, 1993.
22. S.L. Marshall et al. In H.T. MacGillivray et al., editors, *Astronomy From Wide Field Imaging*, *IAU Symp.#161*, 1994.
23. M. Della Valle. *A&A*, 287:L31, 1994.
24. E. Giraud. *IAU Circ.*, (6097 and 6098), 1994.
25. D.P. Bennett et al. In *these proceedings*, 1996.
26. X-P. Wu. *ApJ*, 435:66, 1994.
27. K. C. Sahu. *Nature*, 370:275, 1994.
28. A. De Rujula, G.F. Giudice, S. Mollerach, and E. Roulet. *MNRAS*, 275:545, 1995.
29. J.N. Bahcall, C. Flynn, A. Gould, and S. Kirhakos. *ApJ*, 435:L51, 1994.
30. E.M. Hu, J.S. Huang, G. Gilmore, and L.L. Cowie. *Nature*, 371:493, 1994.
31. C. Flynn, A. Gould, and J.N. Bahcall. *preprint*, 1996. (astro-ph/9603035).
32. B. Carr. *ARA&A*, 32:531, 1994.
33. S. Charlot and J. Silk. *ApJ*, 445:124, 1996.
34. S.D.M. White, J.F. Navarro, A.E. Evrard, and C.S. Frenk. *Nature*, 366:429, 1993.
35. B.D. Fields, G. Mathews, and D.N. Schramm. *preprint*, 1996. (astro-ph/9604095).
36. J. Liebert, C.C. Dahn, and D.G. Monet. *ApJ*, 332:891, 1988.
37. G. Chabrier, L. Segretain, and D. Méra. *preprint*, 1996. (astro-ph/9606083).
38. A. Gould. *ApJ*, 441:L21, 1995.